Generalized Energy-Conserving Dissipative Particle Dynamics with Reactions

Martin Lísal,[1,2] James P. Larentzos,[3] Josep Bonet Avalos,[4] Allan D. Mackie[4] and John K. Brennan[3*]

[1]Department of Molecular and Mesoscopic Modelling, The Czech Academy of Sciences, Institute of Chemical Process Fundamentals, Prague 165 01, Czech Republic
[2]Department of Physics, Faculty of Science, Jan Evangelista Purkyně University in Ústí nad Labem, Ústí n. Lab. 400 96, Czech Republic
[3]U.S. Army Combat Capabilities Development Command (DEVCOM) Army Research Laboratory, Aberdeen Proving Ground, MD 21005, USA
[4]Departament d'Enginyeria Química, ETSEQ, Universitat Rovira i Virgili, Tarragona 43007, Spain

Abstract

We present an extension of the generalized energy-conserving dissipative particle dynamics method (J. Bonet Avalos, *et al.*, *Phys Chem Chem Phys,* **2019,** *21*, 24891-24911) to include chemical reactivity, denoted GenDPDE-RX. GenDPDE-RX provides a means of simulating chemical reactivity at the micro- and mesoscales, while exploiting the attributes of density- and temperature-dependent many-body force fields, which include improved transferability and scalability compared to two-body pairwise models. The GenDPDE-RX formulation considers intra-particle reactivity via a coarse-grain reactor construct. Extent-of-reaction variables assigned to each coarse-grain particle monitor the temporal evolution of the prescribed reaction mechanisms and kinetics assumed to occur within the particle. Descriptions of the algorithm, equations-of-motion, and numerical discretization are presented, followed by verification of the GenDPDE-RX method through comparisons to reaction kinetics theoretical model predictions. Demonstrations of the GenDPDE-RX method are performed using constant-volume adiabatic heating simulations of three different reaction models, including both reversible and irreversible reactions, as well as multi-step reaction mechanisms. The selection of the demonstrations is intended to illustrate the flexibility and generality of the method, but are inspired by real material systems that span from fluids to solids. Many-body force fields using analytical forms of the ideal gas, Lennard-Jones, and exponential-6 equations-of-state are used for demonstration, although application to other forms of equation-of-states is possible. Finally, the flexibility of the GenDPDE-RX framework is addressed with a brief discussion of other possible adaptations and extensions of the method.

Keywords: chemical reactivity, coarse-grain models, dissipative particle dynamics, microscale and mesoscale modeling

*corresponding author (john.k.brennan.civ@army.mil)

1. Introduction

Nearly all materials and processes, whether natural or synthetic, are innately heterogeneous, where the heterogeneity is manifested at the microscale. Moreover, while chemical reactivity is intrinsically an atomistic scale event, the initiation of chemistry often stems from mechanisms occurring at the microscale (*e.g.*, microstructural changes, diffusion, or mixing). As the central science, chemistry can be the pivotal driver in such microscale mechanisms, where in all but the simplest reactive systems, the macroscopic properties are effectuated from these multiscale processes. Examples of chemistry dictating the microscale-dependent response can be found in both natural processes (*e.g.*, cell chemistry, atmospheric chemistry, and colloid chemistry) and synthetic processes (*e.g.*, fuel cell chemistry, material manufacturing, tissue engineering, and drug delivery).

Microscale modeling and simulation is a vital component for improving and understanding existing microscale materials and processes, as well as developing novel materials. However, modeling microscale behavior poses many significant challenges. While the spatial and temporal scales preclude the use of atomistic simulation, at the continuum scale, the microscale effects are necessarily homogenized such that they are only resolved in an average manner. Discrete coarse-grain (CG) particle modeling and simulation are capable of filling this gap in computational length scales; accordingly, it is an ever-growing computational research area. A plethora of discrete CG particle modeling studies of micro- and mesoscale phenomena can be found in the literature. Studies have been performed over an extensive scope of materials and applications, including the life sciences (proteins, colloidal suspensions, bio-membranes, micelles), industrial applications (surfactants, asphaltenes, viscoelastic fluids), defense applications (energetic material composites, liquid propellants), and novel materials (self-assembled block copolymers and nanoparticles).[1-18]

For these and other discrete CG particle studies, dissipative particle dynamics (DPD) has demonstrated to be a valuable method. Based on a rigorous statistical mechanics foundation,[19-21] the family of DPD methods allows for simulations under isothermal, isobaric (DPDP),[22-23] isoenergetic (DPDE),[24-26] or isoenthalpic (DPDH)[27] conditions. Further, a method for simulating chemical reactivity exists that was built upon the DPDE framework, notated as DPD-RX.[8, 16, 28] DPD-RX treats the CG particles as interacting CG reactors, where reaction progress variables are assigned to each CG particle that monitor the time evolution of an extent-of-reaction associated with each of the prescribed reactions that may occur within each CG particle. Changes in the chemistry of a reacting CG particle coincide with changes in the particle's interaction potential. Moreover, the particle interaction changes in such a way that it captures both heat exchange and pressure volume work due to the chemical reactivity. To date, the DPD-RX method has been applied to the simulation of the decomposition of energetic materials.[8, 11, 15-16, 28-31]

A more recent DPD method advancement is the generalization of the DPDE method (GenDPDE),[14, 32] which can incorporate density- and temperature-dependent interaction potentials, *e.g.*, a many-body force field based on an analytical equation-of-state (MB-FF-EoS).[33-37] MB-FF-EoS CG models overcome the lack of both scaling consistency and transferability that hinder the use of purely pairwise force fields. In recent work, a detailed derivation of the GenDPDE

equations-of-motion were formulated in a bottom-up manner, preserving a direct link to the higher resolution scale.[14, 32]

In light of these two recent extensions of the DPDE method, namely DPD-RX and GenDPDE, an extension of the GenDPDE method to include chemical reactivity intuitively follows and is presented in this work. Notated as GenDPDE-RX, the extension is based on the isoenergetic version of the DPD-RX method (DPDE-RX), which considers intra-particle reactivity via a coarse-grain reactor construct. Analogous to the DPDE-RX approach, reaction progress variables are assigned to each particle that monitor the time evolution of an extent-of-reaction associated with the prescribed reaction mechanisms and kinetics, assumed to occur within the particle, and coupled to particle state variables, such as the temperature and pressure. The GenDPDE-RX method provides a means of simulating chemical reactivity while utilizing the attributes of density- and temperature-dependent many-body force fields.

The manuscript is organized as the following. In Section 2, the GenDPDE-RX method is presented, including descriptions of the algorithm and numerical discretization. In Sections 3 and 4, details of the reaction models and computational aspects are presented. Sections 5 and 6 provide verification and demonstrations of the GenDPDE-RX method by performing constant-volume adiabatic heating simulations of various types of reaction models, and through comparisons to theoretical model predictions of the reaction kinetics. Finally, a discussion of other possible adaptations and extensions of the GenDPDE-RX method is given.

2. Methodology

A. Algorithm

The extension of GenDPDE to include chemical reactivity is constructed upon the DPDE-RX method,[16] whereby the CG particles are treated as seemingly interacting *coarse-grain reactors* (CG-reactors). The CG-reactor model differs from a reactive-type model in which chemical bonds are explicitly present. Rather, temporal changes in the species type and concentration of the molecules representing the CG particle can occur. As such, the interaction between CG particles varies as reactions proceed during the simulation. These intra-particle changes in chemistry are governed by a prescribed set of chemical reactions and kinetics (termed here as the *reaction model*) and the associated extents-of-reaction. Within each time step, it is assumed that for any composition change within a CG particle, complete species mixing has occurred and the equilibrium reactions reached their steady-state compatible with the actual state variables of the mesoparticle. Schematics of the CG-reactor depiction for the reactions considered in the main text are shown in Figure 1. The total energy of a given particle remains constant during the update of the particle internal energy, which occurs when the composition of the CG particle changes due to reaction. Variations in the CG particle composition are reflected through a CG particle equation-of-state (CG-EoS), which defines the thermodynamics of the internal state of the particle, *i.e.*, the degrees-of-freedom that are not reflected by the explicit particle interactions. The form of the CG-EoS is a modeling choice, where a wide variety can be considered. For example, assuming that

the internal degrees-of-freedom are purely harmonic, the particle internal energy u_i and particle temperature θ_i can be related through a constant-volume heat capacity $C_{V,i}$, as $u_i = C_{V,i}\theta_i$. More advanced CG-EoS forms can incorporate temperature dependence in the parameters as $C_{V,i}(\theta_i)$, or quantum contributions that provide a more accurate description of the high frequency modes.[38] In this work, the CG-EoS is defined as

$$u_i(\theta_i) = \Delta H_{f,i}(T_r) + \int_{T_r}^{\theta_i} C_{P,i}^0(T)dT - \mathcal{N}_{mol}k_B\theta_i - \frac{3}{2}k_B\theta_i \tag{1}$$

where T_r is a reference temperature, albeit arbitrary, and

$$\begin{aligned} \Delta H_{f,i}(T_r) &= \sum_{\alpha=1}^{N_s} f_i^\alpha \Delta H_{f,\alpha}(T_r) \\ C_{P,i}^0(\theta_i) &= \sum_{\alpha=1}^{N_s} f_i^\alpha C_{P,\alpha}^0(\theta_i) \\ \mathcal{N}_{mol} &= \sum_{\alpha=1}^{N_s} \mathcal{N}_i^\alpha \end{aligned} \tag{2}$$

In Eqs. (1) and (2), N_s is the number of species types embedded within particle i, f_i^α is the fraction of species α within particle i, $\mathcal{N}_i^\alpha$ is the number of particles of species α embedded within mesoscopic particle i, $\Delta H_{f,\alpha}(T_r)$ is the heat of formation of species α at reference temperature T_r (typically $T_r = 298.15$ K), $C_{P,\alpha}^0(\theta_i)$ is the isobaric heat capacity of an isolated molecule of species α at reference pressure P_r (typically $P_r = 1$ bar), and k_B is the Boltzmann constant. Updates of u_i due to composition changes result in changes in θ_i, which reflect either the exothermic or endothermic behavior of the reaction model. In the GenDPDE-RX method, the reaction volume, $\mathcal{V}_{i,rxn}$, is equivalent to the volume of the particle, $\mathcal{V}_i = \frac{1}{n_i}$, where

$$n_i = \frac{\sum_{j\neq i} w_{ij}}{[w]} \tag{3}$$

is the local density of particle i; $w_{ij} \equiv w(r_{ij})$ is a smooth, non-negative, monotonically decreasing, spherically-symmetric weighting function vanishing for $r_{ij} \geq R_c$; R_c is the cut-off radius and $[w] = 4\pi \int w(r)r^2 dr$.

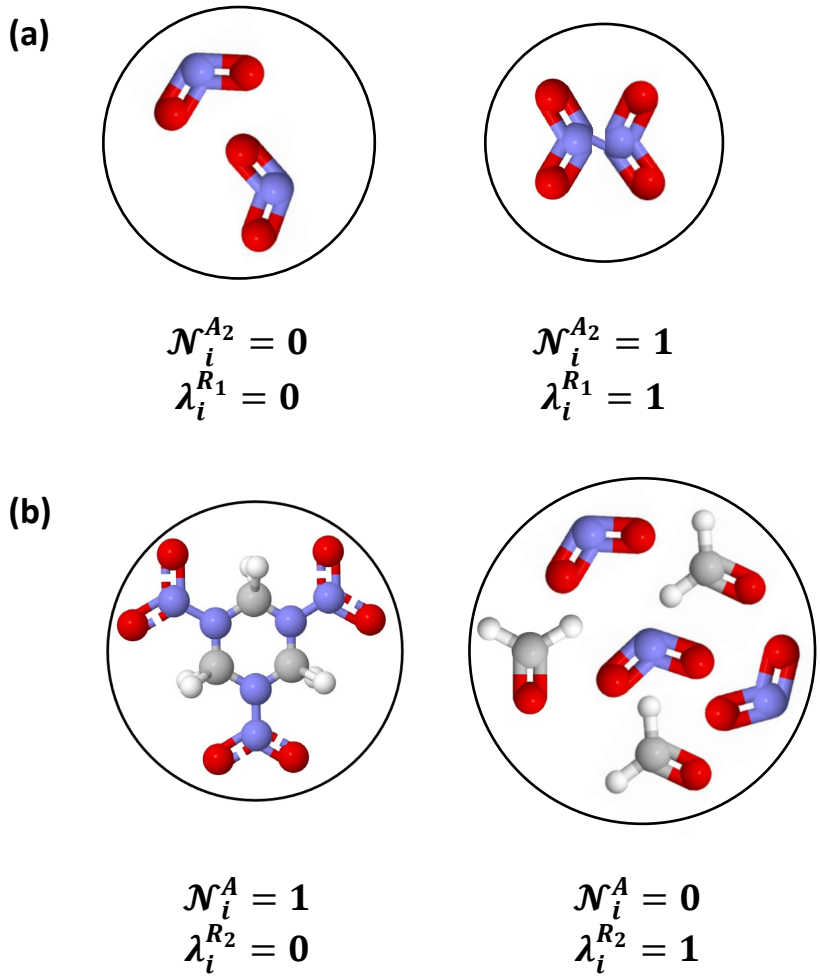

Figure 1: Schematics of the CG-reactor end states for (a) R_1, $2A \rightleftharpoons A_2$; and (b) R_2, $A \rightarrow 3B + 3C$. N_i^{α} is the number of species α within CG particle i and $\lambda_i^{R_x}$ is the extent-of-reaction for Reaction R_x.

B. Equations-of-Motion and Numerical Discretization

The GenDPDE-RX method is built upon the GenDPDE and DPDE-RX frameworks, where the equations-of-motion (EoM) are taken as a combination of the EoM from the two methods. The complete set of EoM for GenDPDE-RX is taken as the GenDPDE EoM accompanied by an update of the particle internal energy due to changes in the particle composition resulting from reaction. An alternative heat flow model has been introduced recently for the GenDPDE method,[32] which was used here.

For particle $(i = 1, \ldots, N)$, the EoM for the GenDPDE method are:

$$\mathbf{r}_i' = \mathbf{r}_i + \frac{\mathbf{p}_i}{m_i}\delta t \tag{4}$$

$$\mathbf{p}_i' = \mathbf{p}_i + \sum_{j \neq i} \mathbf{f}_{ij}^{C}\,\delta t + \sum_{j \neq i} \mathbf{f}_{ij}^{D}\,\delta t + \sum_{j \neq i} \delta \mathbf{p}_{ij}^{R} \tag{5}$$

$$u_i' = u_i - \frac{1}{2}\sum_{j\neq i}\left(\frac{\mathbf{p}_i}{m_i} - \frac{\mathbf{p}_j}{m_j}\right)\cdot \mathbf{f}_{ij}^C\,\delta t - \frac{1}{2}\sum_{j\neq i}\left(\frac{\mathbf{p}_i}{m_i} - \frac{\mathbf{p}_j}{m_j}\right)\cdot \mathbf{f}_{ij}^D\,\delta t - \frac{1}{2}\sum_{j\neq i}\left(\frac{\mathbf{p}_i}{m_i} - \frac{\mathbf{p}_j}{m_j}\right)\cdot \delta\mathbf{p}_{ij}^R - \frac{1}{2m_i}\sum_{j\neq i}\sum_{k\neq i}\delta\mathbf{p}_{ij}^R\cdot\delta\mathbf{p}_{ik}^R + \sum_{j\neq i}\dot{q}_{ij}\,\delta t + \sum_{j\neq i}\delta u_{ij}^R \tag{6}$$

where primed variables refer to the final state at $t+\delta t$, and non-primed variables refer to the initial state at time t; δt is the timestep, m_i, $\mathbf{r}_i$, $\mathbf{p}_i$, and u_i are, respectively, the particle mass, position, momentum, and internal energy. In Eqs. (5) and (6), the interactions between particles i and j are the following:

$$\mathbf{f}_{ij}^C = -\left(\frac{\pi_i^{ex}}{n_i^2} + \frac{\pi_j^{ex}}{n_j^2}\right)\frac{w_{ij}'}{[w]}\boldsymbol{e}_{ij} \tag{7}$$

is the conservative force,

$$\mathbf{f}_{ij}^D = -\gamma_{ij}\mathbf{e}_{ij}\cdot\left(\frac{\mathbf{p}_i}{m_i} - \frac{\mathbf{p}_j}{m_j}\right)\mathbf{e}_{ij} \tag{8}$$

is the dissipative force,

$$\dot{q}_{ij} = -\kappa_{ij}(\theta_i - \theta_j) \tag{9}$$

is the heat flow,

$$\delta\mathbf{p}_{ij}^R = \sqrt{k_B(\theta_i+\theta_j)\gamma_{ij}}\,\xi_{ij}\mathbf{e}_{ij}\delta t^{\frac{1}{2}} \tag{10}$$

is the random contribution to the momentum with $\delta\mathbf{p}_{ij}^R = -\delta\mathbf{p}_{ji}^R$, and

$$\delta u_{ij}^R = \sqrt{2k_B\theta_i\theta_j\kappa_{ij}}\,\bar{\xi}_{ij}\delta t^{\frac{1}{2}} \tag{11}$$

is the random heat exchange with $\delta u_{ij}^R = -\delta u_{ji}^R$. In Eqs. (4) to (11), $r_{ij} = |\mathbf{r}_{ij}|$, $\mathbf{r}_{ij} = \mathbf{r}_i - \mathbf{r}_j$, $\mathbf{e}_{ij} = \mathbf{r}_{ij}/r_{ij}$, $\gamma_{ij} = \gamma\omega_{ij}$, $\kappa_{ij} = \kappa\bar{\omega}_{ij}$, $\omega_{ij} = \omega\left(\frac{r_{ij}}{R_c^D}\right)$ and $\bar{\omega}_{ij} = \bar{\omega}\left(\frac{r_{ij}}{\bar{R}_c}\right)$ are weighting functions of the distance between the particles with radial cut-offs R_c^D and $\bar{R}_c$, γ is the friction coefficient, κ is the thermal conductivity coefficient, and ξ_{ij} and $\bar{\xi}_{ij}$ are normalized Gaussian random numbers. $\pi_i^{ex} = \pi_i - k_B\theta_i n_i$ is the excess particle pressure, where π_i is the functional form of the pressure that arises from the selected MB-FF-EoS. The distinction between π_i and π_i^{ex} is introduced to ensure that the MB-FF-EoS faithfully reproduces the macroscopic EoS. This difference arises from the motion of the mesoparticles themselves, which account for the ideal gas contribution ($\pi_i^{IG} = k_B\theta_i n_i$) to the system pressure.

These GenDPDE EoM are accompanied by an update of the particle internal energy due to changes in the particle composition resulting from chemical reactions. During the reaction step, it is assumed that the total energy of the system remains constant. The particle compositions are

updated based on the reaction rate-law model, which subsequently requires updates of the particle internal energies and particle temperatures.

The numerical integration of the EoM given in Eqs. (4) to (6) was performed using an extended Shardlow-splitting algorithm developed previously,[14] while numerical solution of the reaction model follows the original DPDE-RX method.[16] The complete numerical discretization of the EoM and numerical solution of the reactive component of the GenDPDE-RX method are given in Section S.2 of the Supporting Information. Lastly, a list of the key symbols used in the manuscript is provided in Section S.3 of the Supporting Information.

C. Brief comparison between GenDPDE-RX and DPDE-RX

A brief discussion comparing the GenDPDE-RX and DPDE-RX methods is worthwhile here. In accounting for chemical reactivity, both methods are formulated upon the CG-reactor construct, which is merely a computational means of depicting the reactivity occurring within the local volume of the CG particle. In both methods, reaction progress variables are assigned to each particle that monitor the time evolution of an extent-of-reaction associated with the prescribed set of chemical reaction mechanisms and kinetics defined in the reaction model. It is assumed that for any change in chemistry that occurs within a CG particle, the species mixing is instantaneous, and the internal state of the particle, including the internal chemical potential, is further assumed equilibrated. Likewise, in both methods mass exchange between CG particles does not occur during the reaction step; moreover, the total energy of a given particle does not change either. Both methods exhibit both heat-exchange and pressure-volume work, which occur due to chemical reactivity, although through slightly different mechanisms. Finally, both methods maintain total linear and angular momenta, preserve Galilean invariance, and conserve total energy.

In the context of comparing the general frameworks of GenDPDE and DPDE that the GenDPDE-RX and DPDE-RX methods themselves are built upon, a key advantage of GenDPDE is the integration of temperature-dependent interaction potentials, which is not viable in DPDE.[14, 32] As mentioned previously, temperature-dependent interaction potentials provide improved transferability and scalability compared to two-body pairwise models. Moreover, key differences related to the treatment of chemical reactivity exist between the GenDPDE-RX and DPDE-RX methods, where one such difference is in the treatment of the stored chemical energy released or absorbed during reaction, *i.e.*, the heat of reaction. For either method, the heat of reaction is reflected in the observed changes in the particle temperature θ_i. However, in the GenDPDE-RX method, the particle temperature θ_i appears in both the conservative force $\mathbf{f}_{ij}^{C}$ and the CG-EoS, while in DPDE-RX, θ_i appears in only the CG-EoS. As such, the heat of reaction is manifested differently in the methods. Another key difference is that the reaction volume, $\mathcal{V}_{i,rxn}$ in the GenDPDE-RX method is equivalent to the volume of the particle, $\mathcal{V}_i$, which is a function of the particle positions and varies during the simulation. In contrast, within the DPDE-RX framework, a direct physical equivalence does not exist between these two quantities, as the particles are regarded as constant-volume reactors. As such, several approaches for defining $\mathcal{V}_{i,rxn}$ are possible within the DPDE-RX framework and ultimately is a modeling choice, albeit a choice that can significantly influence the reaction rate.[16] Finally, explicit values of the particle chemical potential are readily available in the GenDPDE-RX framework via the MB-FF-EoS, which are not available

from the DPDE-RX method. The accessibility of these values may be convenient when considering implementing alternative modeling forms of the reaction model or performing additional analysis (*cf.* Section 5).

3. Models

For demonstration of the GenDPDE-RX method, three different reaction models are considered: (R_1) a reversible, dimerization reaction, $2A \rightleftharpoons A_2$; ($R_2$) a unimolecular, irreversible, exothermic decomposition reaction, $A \rightarrow 3B + 3C$; and (R_3) a unimolecular, four-step decomposition reaction, which has been previously studied using the DPD-RX method.[16] Further details along with the demonstrations of R_3 are presented in Section S.1 of the Supporting Information. The reaction models are presented here in a general fashion to illustrate the flexibility and robustness of the GenDPDE-RX framework. However, these reaction models and the chemical species models are inspired by realistic systems that are physically meaningful and span a range of phase behavior from fluids to solids. Lastly, for simplicity the reaction models considered in this work are purely deterministic, rather than stochastic in nature. Stochastic reaction models, which are commonly found in theoretical stochastic processes,[39] consider both the deterministic reaction laws and the mesoscopic fluctuations about them. Implementing stochastic reaction models within the GenDPDE-RX framework may be considered in the future.

For the reversible, dimerization reaction (R_1), the rate laws for the forward (fwd) and reverse (rev) reactions are defined as:

$$\begin{aligned} d[A] &= -2k_{R_1}^{fwd}[A]^2 dt + 2k_{R_1}^{rev}[A_2]dt \\ d[A_2] &= k_{R_1}^{fwd}[A]^2 dt - k_{R_1}^{rev}[A_2]dt \end{aligned} \tag{12}$$

while the rate laws for the unimolecular, irreversible decomposition reaction (R_2) are defined as:

$$\begin{aligned} d[A] &= -k_{R_2}[A]dt \\ d[B] &= d[C] = 3k_{R_2}[A]dt \end{aligned} \tag{13}$$

In Eqs. (12) and (13), k_{R_x} is the reaction rate constant of reaction R_x, $[\alpha] = \frac{\mathcal{N}_i^\alpha}{\mathcal{V}_i}$ is the concentration of species α within particle i, $\mathcal{N}_i^\alpha$ is the number of particles of species α embedded within particle i, and $\mathcal{V}_i$ is the reaction volume associated with particle i, both defined above. For each CG particle, each reaction rate law can be re-written in terms of an extent-of-reaction, $\lambda_i^{R_x} = \frac{\mathcal{N}_i^\alpha - \mathcal{N}_i^{\alpha,0}}{\nu_\alpha}$, where $\mathcal{N}_i^{\alpha,0}$ is the initial number of species α within particle i, and ν_α is the stoichiometric coefficient of species α. Each reaction rate constant k_{R_x} is modeled by an Arrhenius expression

$$k_{R_x} = A_{R_x} exp\left(-\frac{E_{R_x}}{k_B \overline{\theta}_i}\right) \tag{14}$$

where A_{R_x} is the Arrhenius pre-factor, E_{R_x} is the activation energy, and $\overline{\theta}_i$ is defined as a Lucy-weighted local-average particle temperature of CG particle i, which includes the neighboring particles of i and itself. For consistency with the GenDPDE algorithm,[14, 32] an arithmetic average of $\overline{\theta}_i$ is used. The form of $\overline{\theta}_i$ is a modeling choice, where alternative forms of $\overline{\theta}_i$ can be considered, but keeping with the spirit of the GenDPDE framework, a form that considers neighboring particles is recommended. The use of $\overline{\theta}_i = \theta_i$ is not recommended due to potentially large fluctuations in the instantaneous value of θ_i.

The internal state of the particles is modeled using the ideal gas (IG) EoS, for reaction model R_1, and an analytical EOS for the Lennard-Jones (LJ) fluid, for reaction model R_2. The LJ EoS developed by Kolafa and Nezbeda[40] was implemented, which produces results of high accuracy, when compared to the simulated ones, for both the pressure and internal energy over a wide range of temperatures and densities. Analogous to the DPD-RX method,[16] the mixture within a CG particle is modeled using the van der Waals one-fluid (vdW-1f) approximation.[41-43] The composition-dependent LJ parameters are determined in typical fashion as[43-44]

$$\begin{aligned} \sigma_m^3 &= \sum_a \sum_b x_a x_b \sigma_{ab}^3 \\ \varepsilon_m &= \frac{1}{\sigma_m^3} \sum_a \sum_b x_a x_b \varepsilon_{ab} \sigma_{ab}^3 \end{aligned} \tag{15}$$

ε_m and σ_m are the LJ energy and size parameters, respectively, x_a and x_b are mole fractions of species a and b, respectively, which comprise the mixture, defined within each particle, while $\varepsilon_{ab} = \sqrt{\varepsilon_{aa}\varepsilon_{bb}}$ and $\sigma_{ab} = \frac{\sigma_{aa}+\sigma_{bb}}{2}$. For reaction model R_2, the change in the level of coarse-graining was considered as the reactions proceeded. The CG resolution was adjusted through the local density term used in the many-body interaction potential, where details can be found elsewhere.[37]

4. Computational Details

All simulations utilized the Large-scale Atomic/Molecular Massively Parallel Simulator (LAMMPS)[45] with modifications to the USER-DPD add-on package,[8, 12, 27, 30, 46] and were performed on a three-dimensional system of 8,000 particles, where periodic boundary conditions were imposed in all directions, using a time step of 5.0 fs. A quadratic weighting function was used in the local density model, while the weighting function $\left(1 - \frac{r_{ij}}{R_c}\right)^2$ was used for the friction term and the heat exchange term. The weighting functions of the friction and heat exchange terms vanish beyond a spherical cutoff radius, R_c, $r_{ij} > R_c$, where $R_c = R_c^D = \bar{R}_c = 16.0$ Å. For all

cases, the friction coefficient $\gamma = 0.02\ \frac{eV \cdot ps^{1/2}}{\text{Å}}$ and the heat conductivity coefficient $\kappa = 0.0001\ \frac{eV \cdot K}{ps}$ were used.

5. Verification of the GenDPDE-RX Framework

For verification of the GenDPDE-RX method, the R_1 reversible dimerization reaction, $2A \leftrightharpoons A_2$, is considered at a density of ρ = 1.0 g/cm^3 and an initial temperature of T_0 = 300 K. The system consists of 8,000 CG particles initially arranged on a simple cubic lattice. The CG particles are initially indistinguishable (i.e., all CG particles have a molecular weight of 300.061 g/mol and are initialized with an identical chemical composition), where the particle interactions are described through an IG MB-FF-EoS. The chemical kinetics are described through an Arrhenius expression that depends on the chemical affinity (a_r) of the reactants (r) in the forward and reverse reactions

$$k_{R_1} = A_{R_1} exp\left(\frac{a_r - E_0}{k_B \bar{\theta}_\iota}\right) \tag{16}$$

where $a_r = \sum_{\alpha \in r} \nu^\alpha \mu^\alpha$, $\nu^\alpha$is the stoichiometric coefficient of species α, and μ^α is the chemical potential of species α given by the expression

$$\mu^\alpha = \mu_0^\alpha + C_V^\alpha(\bar{\theta}_\iota - T_r) - \bar{\theta}_\iota C_V^\alpha \ln\frac{\bar{\theta}_\iota}{T_r} \tag{17}$$

μ_0^α is the chemical potential of species α at a reference temperature T_r and C_V^α is the constant volume heat capacity of species α. A temperature independent, constant volume heat capacity was used for each species in R_1. The reaction kinetics parameters of the forward and reverse reactions of reaction R_1 are listed in **Table 1** and the thermochemical data of each chemical species is given in **Table 2**.

Table 1: The Arrhenius pre-factor A_{R_1} and the energy barrier E_0 for the reversible dimerization reaction R_1, as described by the Arrhenius expression given in Eq. (16).

R_1	A_{R_1}	$\frac{E_0}{k_B}$ [K]
R_1^{fwd}: $2A \rightarrow A_2$	$(1.0x10^{13}\ \frac{1}{s}) \cdot \mathcal{V}_i$	12000.1
R_1^{rev}: $A_2 \rightarrow 2A$	$1.0x10^{13}\ \frac{1}{s}$	12000.1

Table 2: Thermochemical data for reversible dimerization reaction R_1.

Species	$\frac{\Delta H_f^0}{k_B}$ [K] [a]	$\frac{C_V}{k_B}$	μ_0 [K] [a]

A [NO]	10854.6	15.0	5129.1
A_2 [$(NO)_2$]	20279.0	30.0	9984.6

[a] Heats of formation (ΔH_f^0) and chemical potentials (μ_0) are reported at a reference temperature of $T_r = 298.15$ K.

Particle velocities and particle internal temperatures are randomly assigned from a Maxwell-Boltzmann distribution with a temperature of $T_0 = 300$ K. A 1.0-ns GenDPDE equilibration simulation with velocity rescaling (±25 K window) is conducted in a non-reactive mode (*i.e.*, the chemical compositions of the particles do not evolve with time) to equilibrate the system at $T_0 = 300$ K, followed by a 10-ns GenDPDE-RX non-equilibrium simulation during which the chemistry evolves to steady-state conditions.

The temporal evolution of the internal temperature and the average CG particle extent-of-reaction, $\langle \lambda_i^{R_1} \rangle$, is presented in Figure 2. Three separate GenDPDE-RX simulations with different initial conditions are conducted, where each CG particle i is initialized with the following extents-of-reaction: (Case 1) $\lambda_{i,0}^{R_1} = 0$, (Case 2) $\lambda_{i,0}^{R_1} = 1$, and (Case 3) $\lambda_{i,0}^{R_1} = 0.5$. Cases 1 and 2 correspond to pure reactant and product, respectively. For each case, the systems are shown to converge to an equivalent steady-state extent-of-reaction of $\langle \lambda_i^{R_1} \rangle \approx 0.63$. For Case 1, the system temperature is shown to rise since the forward reaction is favored, which is exothermic. Contrastingly, for Case 2, the endothermic reverse reaction is favored, thus the temperature decreases. For Case 3, the initial condition is near the steady-state chemical composition, thus only a small increase in temperature is observed due to a shift in the forward (exothermic) direction.

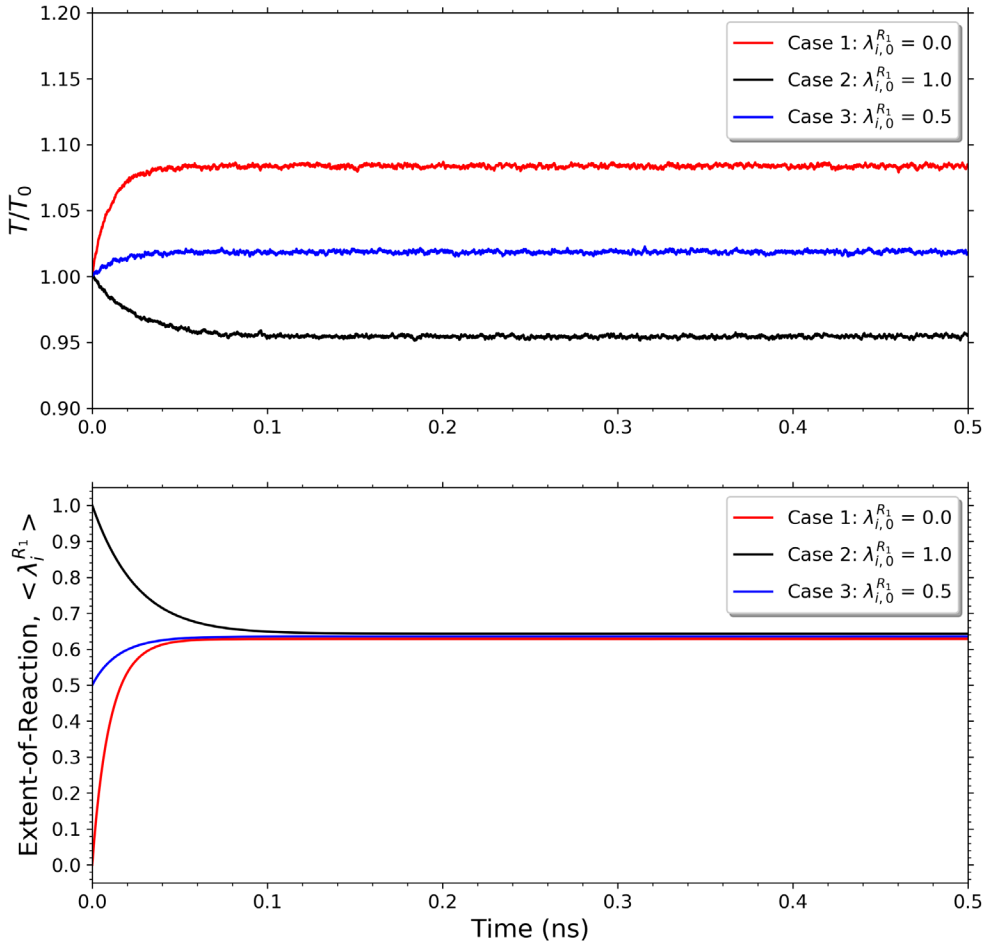

Figure 2: Temporal evolution of the internal temperature and extent-of-reaction using a reversible, dimerization reaction (R_1) at a temperature of 300 K and a density of 1.0 g/cm^3. The different systems were initialized with extents-of-reaction of: (Case 1) $\lambda_{i,0}^{R_1} = 0$, (Case 2) $\lambda_{i,0}^{R_1} = 1$, and (Case 3) $\lambda_{i,0}^{R_1} = 0.5$.

For verification of these results, comparisons are made to the Kramers theory of chemical reaction kinetics, which relates the rate of chemical reaction to the probability of crossing a thermally-activated energy barrier of height, E_0.[47-48] The probability of overcoming the barrier either from the reactant or product state is given by the exponential of the difference between the state and the maximum of the barrier, scaled by $1/(k_B T)$. This leads to the notion of a flow through the energy barrier in the forward direction (reactants to products) J^+ and reverse direction J^-, where specifically for R_1:

$$J^+ = k^+ exp\left(\frac{-a_r - E_0}{k_B \bar{\theta}_i}\right) = k_{R_x} \exp\left(\frac{2\mu^A - E_0}{k_B \bar{\theta}_i}\right) \tag{18}$$

$$J^- = k^- exp\left(\frac{a_p - E_0}{k_B \bar{\theta}_i}\right) = k_{R_x} \exp\left(\frac{\mu^{A_2} - E_0}{k_B \bar{\theta}_i}\right)$$

In Eq. (18), the reactant (r) and product (p) states are characterized by the affinity a_r and a_p defined by $a_r = \sum_{\alpha \in r} \nu^a \mu^\alpha$ and $a_p = \sum_{\alpha \in p} \nu^a \mu^\alpha$, respectively, where ν^a and μ^α are the stoichiometric coefficient and chemical potential of species α, respectively, and k_{R_x} is the equilibrium pre-factor, and the barrier is scaled by $1/(k_B \bar{\theta})$. The balance between J^+ and J^- "drives" the chemical reaction in terms of the extent-of-reaction, λ:

$$\frac{d\lambda}{dt} = J^+ - J^-$$

At equilibrium, $d\lambda/dt = 0$, *i.e.*, $J^+ = J^-$, and since the equilibrium condition cannot depend on the kinetic properties, the forward and reverse pre-factors are, respectively, $k^+ = k^- \equiv k_{R_x}$.

Figure 3 compares the temperature dependence of the extent-of-reaction between the Kramers theoretical model predictions (solid line) and GenDPDE-RX predictions. GenDPDE-RX simulations presented in Figure 2 were repeated at initial temperatures T_0 ranging from 300 K to 800 K using a constant, temperature-independent chemical potential (*i.e.*, $\mu^\alpha = \mu_0^\alpha\ (298\ K)$). Excellent agreement is found between the theoretical and simulation predictions at all temperatures, indicating consistency of the GenDPDE-RX framework. As an additional interesting comparison, GenDPDE-RX simulations at the various temperatures were performed using the instantaneous particle chemical potential. The effect of using a locally-fluctuating, temperature-dependent chemical potential (*cf.* Eq. (17)) is shown in Figure 3 ($\mu = \mu\ (\theta)$). Both the temperature dependence and the local fluctuations in the thermodynamic variables, which are distributions rather than merely scalar quantities in the GenDPDE-RX framework, cause deviations from the constant-temperature theoretical predictions.

As a final note, the treatment of the reaction kinetics based on Kramers theory requires evaluation of μ^α, which can be readily performed in the GenDPDE-RX framework via the mesoparticle thermodynamics.[14, 32] However, in the DPDE-RX framework, an explicit value of μ^α is not available, thus such an analysis is not feasible.[16]

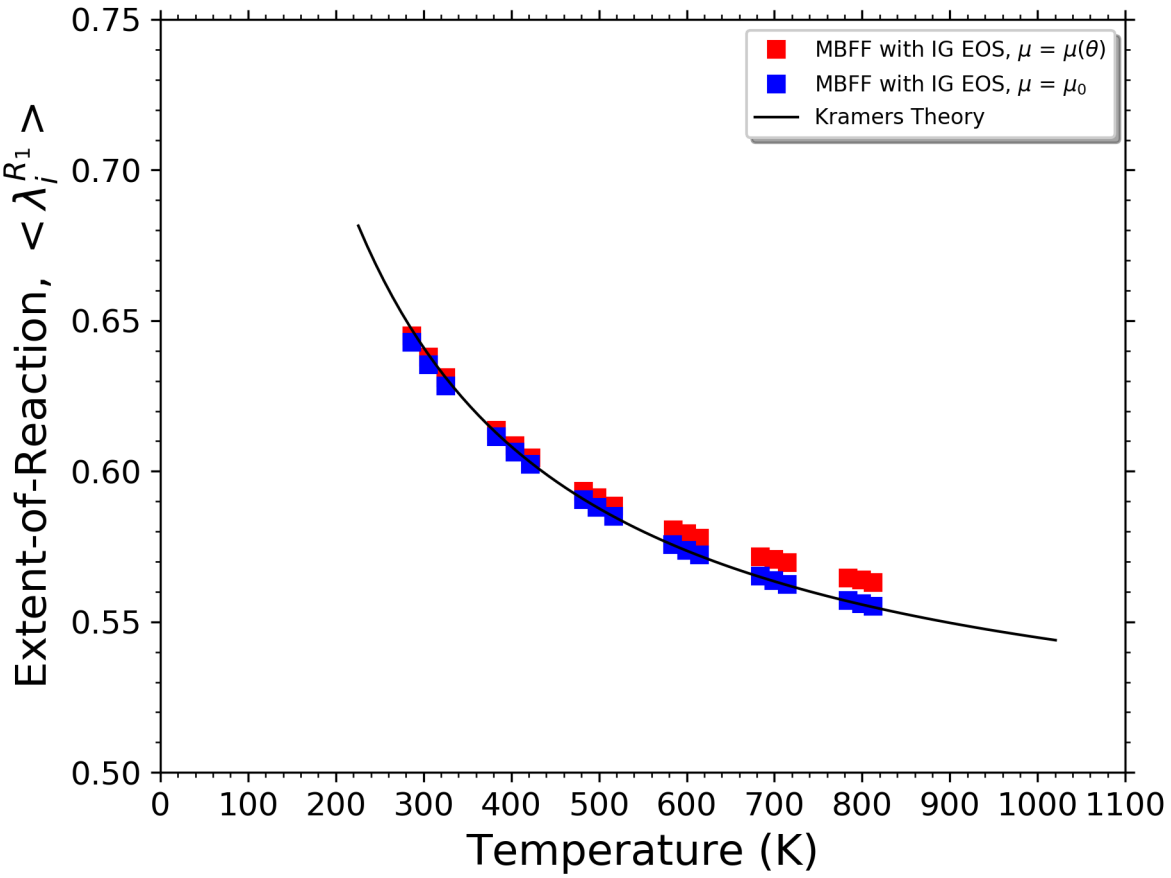

Figure 3: Comparison of the temperature dependence of the extent-of-reaction between the Kramers theoretical model of reaction kinetics (solid line) and GenDPDE-RX for reaction model R_1.

6. Demonstration of the GenDPDE-RX Framework

For demonstration purposes, constant-volume adiabatic flash heating simulations are performed by instantaneously heating all CG particles to a target temperature (T_{heat}), after which no additional energy is added to the system. A unimolecular, irreversible, exothermic decomposition reaction (R_2), $A \rightarrow 3B + 3C$, is considered, where the three molecular species were modeled using an analytical EOS for the Lennard-Jones fluid[40]. For reaction (R_2), an Arrhenius prefactor of $A_{R_2} = 6 \cdot 10^{13} \frac{1}{s}$ and an activation energy of $\frac{E_{Rx}}{k_B} = 18041$ K were used to describe the reaction kinetics. The thermochemical data and LJ fluid parameters for the chemical species in reaction (R_2) are given in Table 3.

Table 3: Thermochemical data and Lennard-Jones fluid parameters, ε_{LJ} and σ_{LJ}, for decomposition reaction R_2.

Species	$\frac{\Delta H_f^0}{k_B}$ [K]	$\frac{C_P}{k_B}$	$\frac{\varepsilon_{LJ}}{k_B}$ [K]	σ_{LJ} [Å]
A [RDX] [b]	23092.3	11th-order polynomial	750.0	6.55
B [CH_2O] [c]	-13939.6	Chebyshev	325.0	3.29
C [N_2O] [c]	9868.4	Chebyshev	217.0	3.80

[b] For Species A, the heat of formation and 11th-order polynomial used for the temperature-dependent heat capacity model are obtained from previous studies involving the RDX molecule[16].

[c] For Species B and C, the heats of formation are obtained from NIST[49] and the temperature-dependent, Chebyshev heat capacity models are obtained from the Cheetah product library[50] for the CH_2O and N_2O molecules, respectively.

The equilibration protocol for generating the initial states consisted of a two-stage decompression-compression process, as described in our previous work.[16] Each of the CG particles are initially indistinguishable with a molecular weight of 222.1 g/mol and a chemical composition $\mathcal{N}^{0,A} = 1.0$. A scheme that prevents numerical instabilities at low and high local densities was used when determining the particle interactions described through the LJ EoS used.[14]

Figure 4 presents the temporal evolution of the kinetic temperature, average particle internal temperature, pressure, and average particle extent-of-reaction evolution for reaction R_2 at two different densities ($\rho = 1.0$ g/cm^3 and 1.8 g/cm^3) and two different flash heating temperatures ($T_{heat} = 1000$ K and 1250 K). Under these conditions, the system changes from an initial melt state, into a high-density fluid phase, until reaching steady-state behavior at supercritical fluid conditions. As the reactant decomposes, an increase in the system pressure is observed due to the multiple product species being formed. Similar to the behavior observed for R_1, steady-state behavior was achieved with simulation times dependent on T_{heat}. A strong dependence on T_{heat} is observed, where the release of chemical energy occurs at time scales that differ by 1-2 orders of magnitude. Additionally, a dependency on the density is observed, where the higher density system results in faster reaction kinetics due to a smaller reaction volume ($\mathcal{V}_{i,rxn}$), mimicking an increase of molecular collisions. The effect of density is manifested through a higher system pressure, while minimal dependence is observed for the temperature profiles. The exothermicity of the reaction model is evident in the temperature profiles, where the continually increasing kinetic temperatures (transparent blue lines) and particle internal temperatures track closely with each other during the entirety of the simulations.

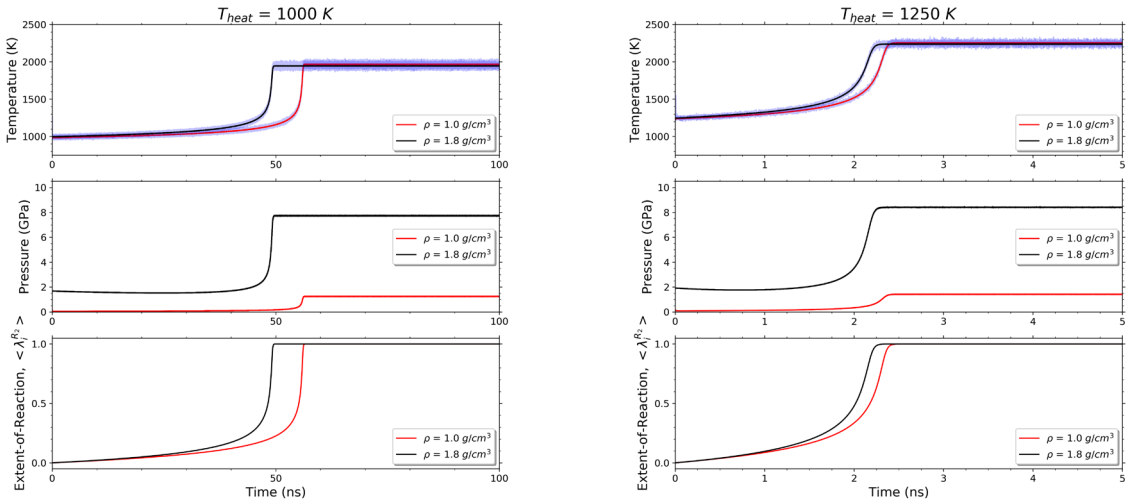

Figure 4: Temporal profiles of the kinetic temperature (transparent blue line), average particle internal temperature (red line), pressure and average particle extent-of-reaction from constant-volume adiabatic flash heating simulations of an irreversible reaction (R_2) model at 1000 K (left frames) and 1250 K (right frames) at densities of 1.0 g/cm^3 and 1.8 g/cm^3.

As a final demonstration of the GenDPDE-RX method, constant-volume adiabatic flash heating simulations were performed for an irreversible four-step decomposition reaction model, where the nine reacting species were modeled using an analytical EoS for the exponential-6 fluid.[51-53] Additional details of the models, simulation set-up, and the resulting temporal profiles can be found in Section S.1 of the Supporting Information.

7. Discussion and Conclusions

As a computational means of investigating the role of chemistry on microscale mechanisms and material microstructure, we extended the generalized energy-conserving dissipative particle dynamics method to include chemical reactivity. The GenDPDE-RX method combines elements of both the GenDPDE[14] and DPDE-RX[16] methods. GenDPDE-RX provides a means of simulating chemical reactivity at the micro- and mesoscales, while exploiting the attributes of density- and temperature-dependent many-body force fields. Analogous to the DPDE-RX method, the GenDPDE-RX formulation considers intra-particle reactivity via a CG reactor construct. Extent-of-reaction variables assigned to each CG particle monitor the temporal evolution of the prescribed reaction mechanisms and kinetics.

Demonstrations of the GenDPDE-RX method were performed using three different reaction models, including reversible and irreversible reactions, and multi-step reaction mechanisms. The choices of the particular reaction models were intended to illustrate the flexibility and generality of the method, but were inspired by real material systems that encompass a wide range of phase space. GenDPDE-RX has a flexible framework such that further adaptations and extensions of the method are possible, including chemistry modeled using reduced or complex reaction

mechanism models. Furthermore, GenDPDE-RX is applicable beyond the EoS considered for the demonstration purposes in this work, including advanced EoS such as the Statistical Associating Fluid Theory (SAFT) EoS,[54] numerically-tabulated EoS, and density-dependent only models.

The version of the GenDPDE-RX method presented here is limited to intra-particle chemical reactivity. Neither inter-particle chemical reactions nor mass diffusion between particles can occur. As such, for the demonstrations presented here, we only considered activation-controlled reactions in homogenous systems. However, the inclusion of reactivity within the mesoscopic description of GenDPDE was a necessary step towards the construction of a complete mesoscopic framework, which includes fluctuating reactions within particles of variable composition, together with mass transport between particles. Work is planned to extend the GenDPDE-RX framework to include mass transfer between particles, which within such a framework, diffusion-limited reactions could be simulated. The ability to simulate diffusive mass transport using GenDPDE-RX would be valuable for a wide range of heterogeneous systems such as shocked composites,[15-16,28-31] flame front propagation,[55] and fuel combustion, among many other possible applications. Subsequently, fundamental reaction kinetic principles[56-57] can be used for straightforward application of the method to a wider range of reacting systems, *e.g.*, combination reactions, $A + B \leftrightharpoons C + D$, or conformational transitions, $A_1 \leftrightharpoons A_2$. For these additional reacting systems, in particular the latter, mass transfer via diffusion can play a dominant role. Lastly, further future work on the GenDPDE-RX method will include a study of the dependence of the level of coarse graining on the thermodynamic and transport properties.

Acknowledgements

Research performed by ML was sponsored by the Army Research Office and was accomplished under Cooperative Agreement Number W911NF-20-2-0203. JKB and JPL acknowledge support in part for a grant of computer time from the Department of Defense High Performance Computing Modernization Program at the Army, Navy, and Air Force Supercomputing Resource Centers. Research performed by JBA and ADM was sponsored by the Army Research Office and was accomplished under Cooperative Agreement Number W911NF-20-2-0227.

Disclaimer

Supporting Information

An additional demonstration of GenDPDE-RX, details of the numerical discretization of GenDPDE-RX, and a list of symbols and notation used in the manuscript.

References

1. Venturoli, M.; Maddalenasperotto, M.; Kranenburg, M.; Smit, B., Mesoscopic models of biological membranes. *Phys. Rep.* **2006**, *437* (1-2), 1-54.
2. Brennan, J. K.; Lísal, M., CECAM Workshop: 'Dissipative particle dynamics: addressing deficiencies and establishing new frontiers' (16–18 July 2008, Lausanne, Switzerland). *Molecular Simulation* **2009**, *35* (9), 766-769.
3. Brennan, J. K.; Lísal, M., Coarse-Grain Models for Metals: Constant-Pressure Dissipative Dynamics Simulations. *Proc. of 14th Int. Det. Symp.* **2010**, *Office of Naval Research ONR-351-10-185*, 1451-1459.
4. Moeendarbary, E.; Ng, T. Y.; Zangeneh, M., Dissipative Particle Dynamics in Soft Matter and Polymeric Applications −A Review. *Int. J. Appl. Mech.* **2010**, *02* (01), 161-190.
5. Chennamsetty, N.; Bock, H.; Lísal, M.; Brennan, J. K., An Introduction to Coarse-Graining Approaches: Linking Atomistic and Mesoscales. In *Process Systems Engineering: Vol. 6 Molecular Systems Engineering*, Adjiman, C.; Galindo, A., Eds. Wiley-VCH Verlag GmbH & Co.: KGaA, Weinheim, **2011**.
6. Ghoufi, A.; Emile, J.; Malfreyt, P., Recent advances in Many-Body Dissipative Particles Dynamics simulations of liquid-vapor interfaces. *Eur Phys J E Soft Matter* **2013**, *36* (1), 10.
7. Noid, W. G., Perspective: Coarse-grained models for biomolecular systems. *J. Chem. Phys.* **2013**, *139* (9), 090901.
8. Brennan, J. K.; Lísal, M.; Moore, J. D.; Izvekov, S.; Schweigert, I. V.; Larentzos, J. P., Coarse-Grain Model Simulations of Nonequilibrium Dynamics in Heterogeneous Materials. *J. Phys. Chem. Lett.* **2014**, *5* (12), 2144-9.
9. Anderson, R.; Malfreyt, P.; Noro, M.; Seaton, M.; Warren, P., DPD: Foundations to Applications. *CECAM Workshop Scientific Report* **2014**.
10. Liu, M. B.; Liu, G. R.; Zhou, L. W.; Chang, J. Z., Dissipative Particle Dynamics (DPD): An Overview and Recent Developments. *Archives of Computational Methods in Engineering* **2014**, *22* (4), 529-556.
11. Kroonblawd, M. P.; Sewell, T. D.; Maillet, J. B., Characteristics of energy exchange between inter- and intramolecular degrees of freedom in crystalline 1,3,5-triamino-2,4,6-trinitrobenzene (TATB) with implications for coarse-grained simulations of shock waves in polyatomic molecular crystals. *J. Chem. Phys.* **2016**, *144* (6), 064501.
12. Moore, J. D.; Barnes, B. C.; Izvekov, S.; Lisal, M.; Sellers, M. S.; Taylor, D. E.; Brennan, J. K., A coarse-grain force field for RDX: Density dependent and energy conserving. *J. Chem. Phys.* **2016**, *144* (10), 104501.
13. Espanol, P.; Warren, P. B., Perspective: Dissipative particle dynamics. *J. Chem. Phys.* **2017**, *146* (15), 150901.
14. Bonet Avalos, J.; Lísal, M.; Larentzos, J. P.; Mackie, A. D.; Brennan, J. K., Generalised dissipative particle dynamics with energy conservation: density- and temperature-dependent potentials. *Physical Chemistry Chemical Physics* **2019**, *21* (45), 24891-24911.
15. Barnes, B. C.; Brennan, J. K.; Byrd, E. F. C.; Izvekov, S.; Larentzos, J. P.; Rice, B. M., Toward a Predictive Hierarchical Multiscale Modeling Approach for Energetic Materials. In *Computational Approaches for Chemistry Under Extreme Conditions*, Goldman, N., Ed. Springer International Publishing: Cham, **2019**; pp 229-282.
16. Lísal, M.; Larentzos, J. P.; Sellers, M. S.; Schweigert, I. V.; Brennan, J. K., Dissipative particle dynamics with reactions: Application to RDX decomposition. *J. Chem. Phys.* **2019**, *151* (11), 114112.

17. Barnes, B. C.; Leiter, K. W.; Larentzos, J. P.; Brennan, J. K., Forging of Hierarchical Multiscale Capabilities for Simulation of Energetic Materials. *Propellants, Explos., Pyrotech.* **2020**, *45* (2), 177-195.
18. Posocco, P.; Posel, Z.; Fermeglia, M.; Lísal, M.; Pricl, S., A molecular simulation approach to the prediction of the morphology of self-assembled nanoparticles in diblock copolymers. *Journal of Materials Chemistry* **2010**, *20* (46), 10511-10520.
19. Hoogerbrugge, P. J.; Koelman, J. M. V. A., Simulating Microscopic Hydrodynamic Phenomena with Dissipative Particle Dynamics. *Europhys. Lett.* **1992**, *19* (3), 155-160.
20. Koelman, J. M. V. A.; Hoogerbrugge, P. J., Dynamic Simulations of Hard-Sphere Suspensions Under Steady Shear. *Europhys. Lett.* **1993**, *21*, 363-368.
21. Español, P.; Warren, P., Statistical Mechanics of Dissipative Particle Dynamics. *Europhys. Lett.* **1995**, *30* (4), 191.
22. Jakobsen, A. F., Constant-pressure and constant-surface tension simulations in dissipative particle dynamics. *J. Chem. Phys.* **2005**, *122* (12), 124901.
23. Trofimov, S. Y.; Nies, E. L. F.; Michels, M. A. J., Constant-pressure simulations with dissipative particle dynamics. *J. Chem. Phys.* **2005**, *123* (14), 144102.
24. Bonet Avalos, J.; Mackie, A. D., Dissipative particle dynamics with energy conservation. *Europhys. Lett.* **1997**, *40* (2), 141-146.
25. Español, P., Dissipative particle dynamics with energy conservation. *Europhys. Lett.* **1997**, *40* (6), 631-636.
26. Mackie, A. D.; Bonet Avalos, J.; Navas, V., Dissipative particle dynamics with energy conservation: Modelling of heat flow. *Phys. Chem. Chem. Phys.* **1999**, *1*, 2039-2049.
27. Lísal, M.; Brennan, J. K.; Bonet Avalos, J., Dissipative particle dynamics at isothermal, isobaric, isoenergetic, and isoenthalpic conditions using Shardlow-like splitting algorithms. *J. Chem. Phys.* **2011**, *135* (20), 204105.
28. Maillet, J. B.; Soulard, L.; Stoltz, G., A reduced model for shock and detonation waves. II. The reactive case. *Europhys. Lett.* **2007**, *78* (6), 68001.
29. Maillet, J. B.; Bourasseau, E.; Desbiens, N.; Vallverdu, G.; Stoltz, G., Mesoscopic simulations of shock-to-detonation transition in reactive liquid high explosive. *Europhys. Lett.* **2011**, *96* (6), 68007.
30. Mattox, T. I.; Larentzos, J. P.; Moore, S. G.; Stone, C. P.; Ibanez, D. A.; Thompson, A. P.; Lísal, M.; Brennan, J. K.; Plimpton, S. J., Highly Scalable Discrete-Particle Simulations with Novel Coarse-Graining: Accessing the Microscale. *Mol. Phys.* **2018**, *116* (15-16), 2061-2069.
31. Larentzos, J. P.; Brennan, J. K.; Izvekov, S.; Lísal, M., Understanding the Role of Microstructure in Energetic Material Composites Using Coarse-Grain Modeling and Simulation. *Proc. of 16th Int. Det. Symp.* **2019**, 1080.
32. Bonet Avalos, J.; Lísal, M.; Larentzos, J. P.; Mackie, A. D.; Brennan, J. K., Generalized energy-conserving dissipative particle dynamics revisited: Insight from the thermodynamics of the mesoparticle leading to an alternative heat flow model. *Phys Rev E* **2021**, *103* (6-1), 062128.
33. Pagonabarraga, I.; Frenkel, D., Non-Ideal DPD Fluids. *Molecular Simulation* **2000**, *25* (3-4), 167-175.
34. Pagonabarraga, I.; Frenkel, D., Dissipative particle dynamics for interacting systems. *J. Chem. Phys.* **2001**, *115* (11), 5015.
35. Trofimov, S. Y.; Nies, E. L. F.; Michels, M. A. J., Thermodynamic consistency in dissipative particle dynamics simulations of strongly nonideal liquids and liquid mixtures. *J. Chem. Phys.* **2002**, *117* (20), 9383-9394.

36. Warren, P. B., Vapor-liquid coexistence in many-body dissipative particle dynamics. *Phys. Rev. E: Stat., Nonlinear, Soft Matter Phys.* **2003**, *68* (6 Pt 2), 066702.
37. Larentzos, J. P.; Mansell, J. M.; Lísal, M.; Brennan, J. K., Coarse-grain modelling using an equation-of-state many-body potential: application to fluid mixtures at high temperature and high pressure. *Mol. Phys.* **2018**, *116* (21-22), 3271-3282.
38. Zhou, Y.; Strachan, A., Thermal conduction in molecular materials using coarse grain dynamics: Role of mass diffusion and quantum corrections for molecular dynamics simulations. *J. Chem. Phys.* **2009**, *131* (23), 234113.
39. van Kampen, N. G., *Stochastic processes in physics and chemistry*. Elsevier: Amsterdam, **2007**.
40. Kolafa, J.; Nezbeda, I., The Lennard-Jones fluid: an accurate analytic and theoretically-based equation of state. *Fluid Phase Equilibria* **1994**, *100*, 1-34.
41. Scott, R. L., Corresponding States Treatment of Nonelectrolyte Solutions. *J. Chem. Phys.* **1956**, *25* (2), 193-205.
42. Leland, T. W.; Rowlinson, J. S.; Sather, G. A., Statistical Thermodynamics of Mixtures of Molecules of Different Sizes. *Trans. Faraday Soc.* **1968**, *64*, 1447-1460.
43. Johnson, J. K.; Zollweg, J. A.; Gubbins, K. E., The Lennard-Jones equation of state revisited. *Mol. Phys.* **1993**, *78* (3), 591-618.
44. Ree, F. H., Simple mixing rule for mixtures with exp-6 interactions. *J. Chem. Phys.* **1983**, *78* (1), 409.
45. Plimpton, S., Fast Parallel Algorithms for Short-Range Molecular Dynamics. *J. Comput. Phys.* **1995**, *117* (1), 1-19.
46. Larentzos, J. P.; Brennan, J. K.; Moore, J. D.; Lísal, M.; Mattson, W. D., Parallel implementation of isothermal and isoenergetic Dissipative Particle Dynamics using Shardlow-like splitting algorithms. *Comput. Phys. Commun.* **2014**, *185* (7), 1987-1998.
47. de Groot, S. R. M. P., *Non-equilibrium thermodynamics*. Dover Publications: New York, **1984**.
48. Kramers, H. A., Brownian motion in a field of force and the diffusion model of chemical reactions. *Physica* **1940**, *7* (4), 284-304.
49. Linstrom, P. J.; Mallard, W. G., *NIST Chemistry WebBook*. National Institute of Standards and Technology: Gaithersburg, MD 20899, **2019**.
50. Bastea, S.; Fried, L. E.; Glaesemann, K. R.; Howard, W. M.; Kuo, I.-F. W.; Souers, P. C.; Vitello, P. A. *Cheetah 6.0 User's Manual.*; LLNL-SM-416166; Lawrence Livermore National Laboratory, **2010**.
51. Sun, J.-X.; Wu, Q.; Cai, L.; Jing, F., Analytic equation of state for exponential-six fluid based on the Ross variational perturbation theory and the Percus–Yevick radial distribution function of hard spheres. *Chemical Physics Letters* **2007**, *449* (1), 72-76.
52. Vortler, H. L.; Nezbeda, O.; Lisal, M., The exp-6 potential fluid at very high pressures: computer simulations and theory. *Mol. Phys.* **1997**, *92* (5), 813-824.
53. Lísal, M.; Smith, W. R.; INezbeda, I., Computer simulation of the thermodynamic properties of high-temperature chemically-reacting plasmas. *J. Chem. Phys.* **2000**, *113* (12), 4885-4895.
54. Chapman, W. G.; Gubbins, K. E.; Jackson, G.; Radosz, M., New reference equation of state for associating liquids. *Industrial & Engineering Chemistry Research* **1990**, *29* (8), 1709-1721.

55. Wang, H.; Julien, B.; Kline, D. J.; Alibay, Z.; Rehwoldt, M. C.; Rossi, C.; Zachariah, M. R., Probing the Reaction Zone of Nanolaminates at ~μs Time and ~μm Spatial Resolution. *The Journal of Physical Chemistry C* **2020**, *124* (25), 13679-13687.
56. House, J. E., *Principles of Chemical Kinetics*. Academic Press: London, **2007**.
57. Pilling, M. J.; Seakins, P. W., *Reaction Kinetics*. University Press: **1999**.